

Evaluating K bands for *Nancy Grace Roman Space Telescope* Rest-Frame NIR SN Ia Distances

D. RUBIN^{1,2}

¹*Department of Physics and Astronomy, University of Hawai‘i at Mānoa, Honolulu, Hawai‘i 96822, USA*

²*E.O. Lawrence Berkeley National Laboratory, 1 Cyclotron Rd., Berkeley, CA 94720, USA*

Submitted to PASP

ABSTRACT

Recently, the *Nancy Grace Roman Space Telescope* (*Roman*) Project raised the possibility of adding another filter to *Roman*. Based on the Filter Working Group’s recommendations, this filter may be a K -band filter, extending significantly redder than the current-reddest $F184$. Among other scientific possibilities, this K filter raises the possibility of measuring SNe Ia in the rest-frame NIR out to higher redshifts than is possible with the current filter complement. I perform a simple survey optimization for NIR SN Ia distances with *Roman*, simultaneously optimizing both filter cutoffs and survey strategy. I find that the roughly optimal K band extends from 19,000Å–23,000Å (giving exposure times roughly half that of a 20,000Å–23,000Å K_s filter). Moving the K much redder than this range dramatically increases the thermal background, while moving the K band much bluer limits the redshift reach. Thus I find any large modification reduces or eliminates the gain over the current $F184$. I consider both rest-frame Y band and rest-frame J band surveys. Although the proposed K band is too expensive for a large rest-frame Y band survey, it increases the rest-frame J Figure of Merit by 59%.

Keywords: Surveys, IR telescopes, Space telescopes, Dark energy, Type Ia supernovae

1. INTRODUCTION

The *Nancy Grace Roman Space Telescope* (*Roman*) is a 2.4 meter space telescope designed for coronagraphy and wide-field optical-NIR imaging and slitless spectroscopy scheduled for launch in the mid 2020’s (Spiegel et al. 2015). The *Roman* Wide-Field Instrument (WFI) will observe 0.28 square degrees per pointing with 0.11 pixels. The large field of view (> 200 times that of the *Hubble Space Telescope*, *HST*, Wide-Field Camera 3 IR), infrared sensitivity, and spectroscopic capability make *Roman* a powerful complement to optical cosmological surveys such as that carried out by the Vera C. Rubin Observatory (Ivezić et al. 2019).

One of *Roman*’s cosmological probes is Type Ia supernovae (SNe Ia), to be observed in large (~ 10 ’s of square degrees), cadenced, deep fields (Spiegel et al. 2015; Hounsell et al. 2018). Figure 1 shows that *Roman* WFI will be large enough to capture many SNe Ia at once in a rolling survey above $z \sim 0.6$.

Figure 2 shows the WFI spectral elements (filters, grism and prism), as well as the possible redder filters considered in this work (referred to as “ K ”). Each filter is labeled with its central wavelength in a three-digit code similar to *HST* (e.g., the $F184$ filter has a central wavelength of 1.84 μm). The baselined filter set was chosen to span most of the sensitive wavelength range of the detectors (H4RG’s with a 2.5 μm cutoff); the 2.0 μm cutoff of the reddest baselined filter ($F184$) minimizes thermal background, thus taking advantage of the dark sky possible in space.

Recently, the *Roman* Project raised the possibility of adding another filter to *Roman*. Based on the Filter Working Group’s recommendations, this filter may be a K -band filter, extending significantly redder than the current-reddest $F184$. As SNe Ia are intrinsically more standard in the rest-frame NIR (e.g., Meikle 2000; Krisciunas 2005; Barone-Nugent et al. 2012; Avelino et al. 2019; Mandel et al. 2020) and possibly have lower dust extinction systematic uncertainties, it is useful to investigate using and optimizing this new K -band filter for measuring SNe Ia.

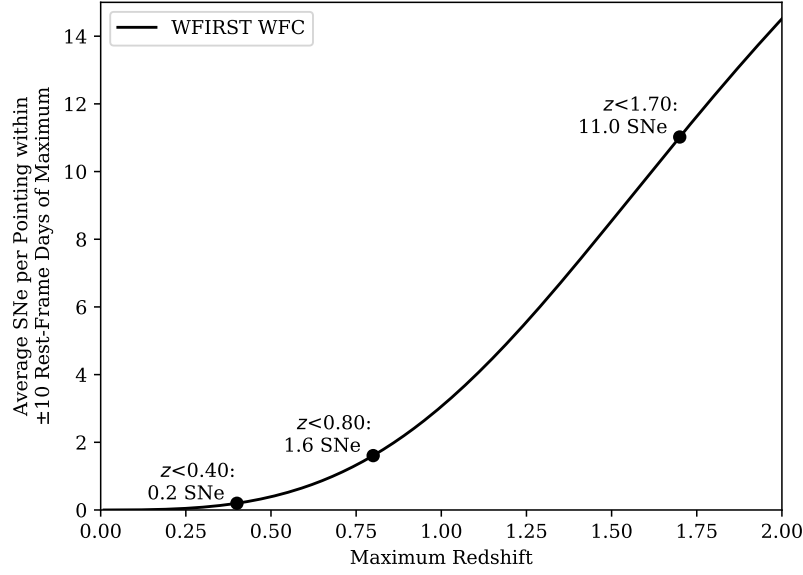


Figure 1. Average number of SNe Ia within 10 rest-frame days of maximum (20 rest-frame day window) in a random WFI pointing as a function of maximum redshift (the distribution is cumulative in redshift). I assume a SN Ia volumetric rate from Rodney et al. (2014). Multiplex is a factor above $z \sim 0.6$ (this value depends on the exact phase range considered useful). Below this redshift, targeted followup observations can improve survey efficiency.

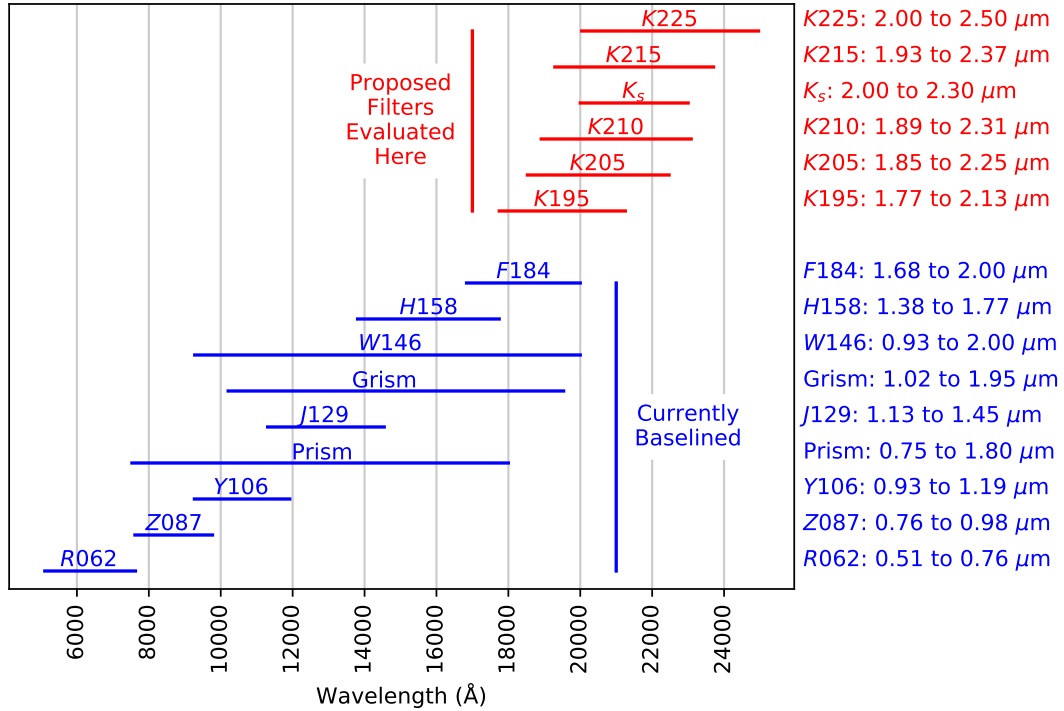


Figure 2. Spectral range of each WFI spectral element (50% on to 50% off). The bottom group shows elements that are currently baselined, while the top group shows possible K filters evaluated in this work.

2. SURVEY SIMULATIONS AND OPTIMIZATION

As much as possible, I make survey simulation assumptions that are likely to be correct in a relative sense, and thus any uncertainties cancel out of the relative FoM/survey optimization. For example, when targeting a certain redshift range, the exposure time is set such that the median SN Ia (on the median host-galaxy background) at the far end of that range has S/N 10 at maximum per 2.5 rest-frame days. This corresponds to a S/N of 10 with a cadence of 5 observer-frame days when targeting $z = 1$, but when targeting $z = 0.4$ (3.6 rest-frame days cadence) a S/N of 12 ($10\sqrt{3.6/2.5}$). If a detailed analysis showed that S/N 8 was a better assumption, the exposure times could be scaled to $\sim (8/10)^2$ while all surveys would contain $\sim (10/8)^2$ or 56% more SNe, but all the surveys would scale the same way relative to each other (except for the nearby SNe Ia and overheads, which are described below). I explicitly verify that the conclusions do not change with total survey time, as discussed below.

By using this same argument that all surveys being optimized scale together, I do not include any source of systematic uncertainties in the forecast. I do note that controlling many sources of systematic uncertainty should be possible, including:

- Photometric nonlinearity in the *K* band, possibly calibratable using lamp-on/lamp-off with the spectral tail of the reddest *Roman* Relative Calibration System LEDs, e.g., [de Jong et al. \(2006\)](#)
- Uncertainties in the NIR SED model for SNe Ia, possibly addressable with a combination of *Roman* prism spectrophotometry, and other programs such as ground-based spectra (e.g., [Hsiao et al. 2019](#)) and space-based spectra (e.g., Supernovae in the Infrared avec Hubble, *HST* GO 15889 PI:Jha)
- Flatfielding uncertainties, especially as most of the thermal emission will be near the filter cutoff wavelength and not near the central wavelength of the filter (see Figure 3). Much of this uncertainty will average out as SNe are distributed randomly over the focal plane.
- Photometric-classification uncertainties (these uncertainties are expected to be small with double-peaked rest-frame NIR SN Ia light curves).
- *K*-band standard-star SED uncertainties, which may be addressable with *James Webb Space Telescope* spectrophotometry.
- Selection effects, which should be small given the high S/N of the light curves (these surveys effectively target a volume-limited sample defined by a given rest-frame NIR range)

Finally, I do not consider alternatives and synergies with NIR light curves for controlling astrophysical systematic uncertainties (e.g., prism spectrophotometry with a SN Ia subclassification approach such as [Fakhouri et al. 2015](#)). A detailed consideration of this is simply beyond the scope of this work.

The survey optimization assumes a Hubble-Lemaître diagram dispersion of 0.12 magnitudes (c.f., [Avelino et al. 2019](#); [Mandel et al. 2020](#)), added in quadrature with $0.055z$ lensing dispersion ([Jönsson et al. 2010](#)), with both dispersions assumed Gaussian. I assume 800 nearby SNe ($0.12/\sqrt{800} = 0.004$ mag) calibrated on the same photometric system as *Roman*. I assume that, given the modest redshifts of these SNe ($z \lesssim 1$), ground-based facilities (e.g., [Takada et al. 2014](#); [DESI Collaboration et al. 2016](#); [de Jong et al. 2014](#)) are able to obtain the redshifts of the host galaxies or live SNe. I compute the Dark Energy Task Force Figure of Merit (DETF FoM, [Albrecht et al. 2006](#)) using a 0.2% CMB shift-parameter constraint assuming a flat universe. This is the same FoM that was used for the SN survey in [Spergel et al. \(2015\)](#).

My survey simulations use a simple pixel-level optimal extraction using WebbPSF *Roman* PSFs ([Perrin et al. 2014](#)). I use 2.55 square meters for the peak effective area of the proposed *K* filters, and the *Roman* Project-supplied effective areas for the other filters.¹ I use the zodiacal background of [Aldering \(2002\)](#), appropriate for a high ecliptic latitude of $\pm 75^\circ$. The supernova fluxes use SALT2-Extended²; the galaxy backgrounds use a model trained on the real backgrounds of high-redshift SNe [Riess et al. \(2007, 2018\)](#), described in more detail in [Rubin et al. \(in prep.\)](#). I assume a conservative $20 e^-$ of read noise per 2.825-second read and a $5 e^-$ floor and a subdominant $0.015 e^-/\text{pixel/s}$

¹ https://roman.gsfc.nasa.gov/science/201907/WFIRST_WIMWSM_throughput_data_190531.xlsm

² 2013 SNANA version called through SNCosmo

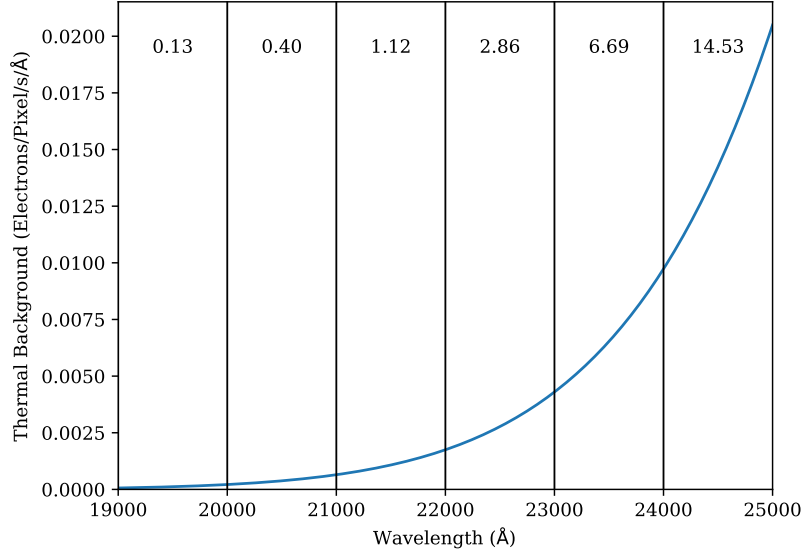


Figure 3. Thermal background (in $e^-/\text{pixel/s}/\text{\AA}$) as described in the text. Also shown is the total in bins of $1,000\text{\AA}$.

of dark + stray-light background.³ The thermal model (which is tuned to produce very similar thermal backgrounds as given by the *Roman* Project) assumes 264K blackbody emission from a combined 2.4 meter primary and secondary mirror with total throughput-weighted emissivity of 0.03. Combined with $10\ \mu\text{m}\ 0''.11$ square pixels (18.75 meter focal length), this gives the model shown in Figure 3.

Table 1 shows how to translate a given redshift distribution of SNe into exposure times. A trial SN survey is specified in terms of the relative number of SNe in each redshift bin. This number of SNe is translated into the areas and depths necessary to measure that many SNe, with any SNe at lower redshift coming for free. I consider surveys measuring at least as red as rest-frame *Y* band ($\lambda \gtrsim 1.04\mu\text{m}$) and surveys measuring at least as red as rest-frame *J* band ($\lambda \gtrsim 1.25\mu\text{m}$). I do not consider rest-frame *H*-band surveys ($\lambda \gtrsim 1.635\mu\text{m}$); even with the reddest practical filters; these would be limited to $z \lesssim 0.4$. Figure 1 shows that these surveys would be more practical with a targeted followup approach (e.g., RAISIN *HST* GO 13046 PI: Kirshner), which is beyond the scope of the rolling surveys considered in this work.

I consider five survey variants for both rest-frame *Y* and rest-frame *J* surveys:

- There is no additional *K*-band filter, so the survey must use the existing *H158* and *F184* filters.
- The optimum *K* filter, which is optimized simultaneously with the survey. For example, a rest-frame *Y* survey targeting a maximum redshift of 1 uses the *K205* filter (see Table 1). The rest-frame wavelength and maximum redshift set the observer-frame central wavelength (with rounding); the filter width around this wavelength is set to maximize S/N (specifically, I maximize filter width/ $\sqrt{\text{thermal background}}$). The *K* filters from Table 1 are shown in the top group of Figure 2.
- I optimize the survey, but the only *K* filter considered is the *K210*. As I show, this filter is roughly optimal for rest-frame *J*-band measurements.
- As above, but using *K215*. This filter is forced to a similar effective wavelength to the *K_s* filter, but has a width chosen to maximize S/N.
- As above, but using *K_s* (the filter proposed by Stauffer et al. 2018).

After computing the relative numbers of pointings required to achieve the SN numbers, I scale the relative numbers to absolute numbers by requiring that the total imaging take 0.2 years or 40% of the total SN survey time (0.5 years).

³ I use a simple quadrature sum of \sqrt{N} Poisson noise and read noise for the noise per pixel, which is not quite accurate (Vacca et al. 2004; Rauscher et al. 2007). I am thus implicitly assuming a more optimal weighting of the detector readouts (e.g., Kubik et al. 2016). However, I am assuming conservative values for the read noise, so this quadrature sum should be achievable with a more detailed treatment.

As described above, my conclusions are not sensitive to the assumption of 0.2 years, as all the surveys scale in the same way with total survey exposure time (I verify this by optimizing surveys with other total times). I also verify that my results are similar with a 260K (rather than 264K) telescope. I optimize each survey with a downhill-simplex code (Nelder & Mead 1965) subject to the constraint that the SNe in each redshift bin must be nonnegative. Downhill-simplex minimization can be challenging even in moderate numbers of dimensions, so I assure convergence by restarting the minimization many times (both in parallel, with randomly chosen starting conditions, and serially, with another maximization started where the previous one terminates).

3. RESULTS AND CONCLUSIONS

Table 2 presents the optimized surveys, filters, and NIR-only FoM values. For the rest-frame *Y* surveys, using *K*195 rather than *F*184 can raise the FoM value 7%. However, *K*195 is not meaningfully redder than the *F*184, and so including *K*195 is hard to justify for a 7% increase. None of the other *K* filters considered supplant the *F*184 (although *K*-band data may be of use for distance cross-checks for a fraction of the SNe observed in the bluer filters, e.g., Dhawan et al. 2018; Burns et al. 2018; Mandel et al. 2020). For the rest-frame *J* surveys, including *K*210 is highly preferred, raising the FoM by 59% compared to an optimized survey without *K*. The *K*215 filter only offers a 26% increase in FoM, and the *K_s* filter only offers a 21% increase in FoM.

For measuring SNe Ia in the NIR, *K*210 thus offers the optimum combination of minimizing thermal background and measuring as red as practical. It is not surprising that the *K*210 filter is significantly more optimal than *K_s*; it gathers $\sim 4/3$ the light (by spanning 19,000Å–23,000Å to the 20,000Å–23,000Å range of *K_s*) with the same level of thermal background (same 23,000Å cutoff), and so needs only $\sim (3/4)^2 = 56\%$ the exposure time.

ACKNOWLEDGMENTS

This work was supported by NASA through grant NNG16PJ311I (Perlmutter *Roman* Science Investigation Team). I acknowledge careful feedback from Greg Aldering, Ben Rose, Susana Deustua, and Rebekah Hounsell.

Software: Astropy (Astropy Collaboration et al. 2013), Mathematica (Wolfram Research Inc. 2020), Matplotlib (Hunter 2007), Numpy (Harris et al. 2020), Python (Van Rossum & Drake 2009), SciPy (Virtanen et al. 2020), SNCosmo (Barbary 2014)

REFERENCES

- Albrecht, A., Bernstein, G., Cahn, R., et al. 2006, arXiv e-prints, astro. <https://arxiv.org/abs/astro-ph/0609591>
- Aldering, G. 2002, doi: [10.2172/842543](https://doi.org/10.2172/842543)
- Astropy Collaboration, Robitaille, T. P., Tollerud, E. J., et al. 2013, A&A, 558, A33, doi: [10.1051/0004-6361/201322068](https://doi.org/10.1051/0004-6361/201322068)
- Avelino, A., Friedman, A. S., Mandel, K. S., et al. 2019, ApJ, 887, 106, doi: [10.3847/1538-4357/ab2a16](https://doi.org/10.3847/1538-4357/ab2a16)
- Barbary, K. 2014, doi: [10.5281/zenodo.592747](https://doi.org/10.5281/zenodo.592747)
- Barone-Nugent, R. L., et al. 2012, MNRAS, 425, 1007, doi: [10.1111/j.1365-2966.2012.21412.x](https://doi.org/10.1111/j.1365-2966.2012.21412.x)
- Burns, C. R., Parent, E., Phillips, M. M., et al. 2018, ApJ, 869, 56, doi: [10.3847/1538-4357/aac51c](https://doi.org/10.3847/1538-4357/aac51c)
- de Jong, R. S., Bergeron, E., Riess, A., & Bohlin, R. 2006, NICMOS count-rate dependent nonlinearity tests using flatfield lamps, Space Telescope NICMOS Instrument Science Report
- de Jong, R. S., Barden, S., Bellido-Tirado, O., et al. 2014, in Society of Photo-Optical Instrumentation Engineers (SPIE) Conference Series, Vol. 9147, Ground-based and Airborne Instrumentation for Astronomy V, ed. S. K. Ramsay, I. S. McLean, & H. Takami, 91470M, doi: [10.1117/12.2055826](https://doi.org/10.1117/12.2055826)
- DESI Collaboration, Aghamousa, A., Aguilar, J., et al. 2016, arXiv e-prints, arXiv:1611.00036. <https://arxiv.org/abs/1611.00036>
- Dhawan, S., Jha, S. W., & Leibundgut, B. 2018, A&A, 609, A72, doi: [10.1051/0004-6361/201731501](https://doi.org/10.1051/0004-6361/201731501)
- Fakhouri, H. K., Boone, K., Aldering, G., et al. 2015, ApJ, 815, 58, doi: [10.1088/0004-637X/815/1/58](https://doi.org/10.1088/0004-637X/815/1/58)
- Harris, C. R., Millman, K. J., van der Walt, S. J., et al. 2020, Nature, 585, 357, doi: [10.1038/s41586-020-2649-2](https://doi.org/10.1038/s41586-020-2649-2)
- Hounsell, R., Scolnic, D., Foley, R. J., et al. 2018, ApJ, 867, 23, doi: [10.3847/1538-4357/aac08b](https://doi.org/10.3847/1538-4357/aac08b)
- Hsiao, E. Y., Phillips, M. M., Marion, G. H., et al. 2019, PASP, 131, 014002, doi: [10.1088/1538-3873/aac961](https://doi.org/10.1088/1538-3873/aac961)

Table 1. Exposure Times and Filters for Median SN as a Function of Maximum Redshift

Maximum		Rest-Frame <i>Y</i> Surveys				Rest-Frame <i>J</i> Surveys			
Redshift	Optimum Filter	<i>K</i> 210	<i>K</i> 215	<i>K_s</i>	Optimum Filter	<i>K</i> 210	<i>K</i> 215	<i>K_s</i>	<i>K_s</i>
0.2	<i>H</i> 158	22.6	<i>H</i> 158	22.6	<i>H</i> 158	22.6	<i>H</i> 158	22.6	<i>H</i> 158
0.3	<i>H</i> 158	39.6	<i>H</i> 158	39.6	<i>F</i> 184	79.1	<i>F</i> 184	79.1	<i>F</i> 184
0.4	<i>H</i> 158	59.3	<i>H</i> 158	59.3	<i>F</i> 184	104.5	<i>F</i> 184	104.5	<i>F</i> 184
0.5	<i>H</i> 158	79.1	<i>H</i> 158	79.1	<i>F</i> 184	141.2	<i>F</i> 184	141.2	<i>F</i> 184
0.6	<i>F</i> 184	194.9	<i>F</i> 184	194.9	<i>K</i> 205	494.4	<i>K</i> 215	1387.1	<i>K_s</i>
0.7	<i>F</i> 184	274.0	<i>F</i> 184	274.0	<i>K</i> 210	1118.7	<i>K</i> 215	1904.1	<i>K_s</i>
0.8	<i>F</i> 184	350.3	<i>F</i> 184	350.3	<i>K</i> 225	7200.9
0.9	<i>K</i> 195	709.1	<i>K</i> 210	2500.1
1.0	<i>K</i> 205	1952.1	<i>K</i> 210	3220.5
1.1	<i>K</i> 215	6378.9
1.2	<i>K</i> 225	17664.7

NOTE—Assumptions for computing required exposure time as a function of maximum redshift in a field. In addition to the exposure times listed above, I assume a 70.625s slew time per pointing (this time is quantized in term of the 2.825s readout time of the WFI detectors, which read and reset during slews for stability and to avoid persistence slewing across bright stars). The left columns show filters and exposure times for surveys that target rest-frame *Y* band; the right columns show surveys that target rest-frame *J* band.

Table 2. Optimized surveys, filter choices, and FoM values

Variant	Rest-Frame <i>Y</i> Surveys				Rest-Frame <i>J</i> Surveys			
No <i>K</i>	25 deg ² <i>H</i> 158 79.1 s, 20 deg ² <i>F</i> 184 350.3 s	267	57 deg ² <i>F</i> 184 141.2s	68	24 deg ² <i>F</i> 184 141.2 s, 6.0 deg ² <i>K</i> 210 1118.7 s	108		
Optimum <i>K</i>	31 deg ² <i>H</i> 158 79.1 s, 9.5 deg ² <i>K</i> 195 709.1 s	285			24 deg ² <i>F</i> 184 141.2 s, 6.0 deg ² <i>K</i> 210 1118.7 s	108		
<i>K</i> 210	25 deg ² <i>H</i> 158 79.1 s, 20 deg ² <i>F</i> 184 350.3 s	267			28 deg ² <i>F</i> 184 141.2 s, 3.1 deg ² <i>K</i> 215 1904.0 s	86		
<i>K</i> 215	25 deg ² <i>H</i> 158 79.1 s, 20 deg ² <i>F</i> 184 350.3 s	267			30 deg ² <i>F</i> 184 141.2 s, 2.6 deg ² <i>K_s</i> 2132.9 s	82		
<i>K_s</i>	25 deg ² <i>H</i> 158 79.1 s, 20 deg ² <i>F</i> 184 350.3 s	267						

NOTE—Results from my optimizations. The first column presents the survey variants I consider: no *K*, a *K* filter that is optimized with the survey strategy, the *K*210 filter, the *K*215 filter, and the *K_s* filter. The next two columns present the optimized survey for each variant and the FoM value for rest-frame *Y* band distances. Finally, the last two columns present the optimized survey for each variant and the FoM value for rest-frame *J* band distances.

- Hunter, J. D. 2007, *Computing in Science & Engineering*, 9, 90, doi: [10.1109/MCSE.2007.55](https://doi.org/10.1109/MCSE.2007.55)
- Ivezić, Ž., Kahn, S. M., Tyson, J. A., et al. 2019, *ApJ*, 873, 111, doi: [10.3847/1538-4357/ab042c](https://doi.org/10.3847/1538-4357/ab042c)
- Jönsson, J., Sullivan, M., Hook, I., et al. 2010, *MNRAS*, 405, 535, doi: [10.1111/j.1365-2966.2010.16467.x](https://doi.org/10.1111/j.1365-2966.2010.16467.x)
- Krisciunas, K. 2005, in *Astronomical Society of the Pacific Conference Series*, Vol. 339, *Observing Dark Energy*, ed. S. C. Wolff & T. R. Lauer, 75
- Kubik, B., Barbier, R., Chabanat, E., et al. 2016, *PASP*, 128, 104504, doi: [10.1088/1538-3873/128/968/104504](https://doi.org/10.1088/1538-3873/128/968/104504)
- Mandel, K. S., Thorp, S., Narayan, G., Friedman, A. S., & Avelino, A. 2020, arXiv e-prints, arXiv:2008.07538. <https://arxiv.org/abs/2008.07538>
- Meikle, W. P. S. 2000, *MNRAS*, 314, 782, doi: [10.1046/j.1365-8711.2000.03411.x](https://doi.org/10.1046/j.1365-8711.2000.03411.x)
- Nelder, J. A., & Mead, R. 1965, *The Computer Journal*, 7, 308, doi: [10.1093/comjnl/7.4.308](https://doi.org/10.1093/comjnl/7.4.308)
- Perrin, M. D., Sivaramakrishnan, A., Lajoie, C.-P., et al. 2014, in *Society of Photo-Optical Instrumentation Engineers (SPIE) Conference Series*, Vol. 9143, *Space Telescopes and Instrumentation 2014: Optical, Infrared, and Millimeter Wave*, ed. J. Oschmann, Jacobus M., M. Clampin, G. G. Fazio, & H. A. MacEwen, 91433X, doi: [10.1117/12.2056689](https://doi.org/10.1117/12.2056689)
- Rauscher, B. J., Fox, O., Ferruit, P., et al. 2007, *PASP*, 119, 768, doi: [10.1086/520887](https://doi.org/10.1086/520887)
- Riess, A. G., Strolger, L.-G., Casertano, S., et al. 2007, *ApJ*, 659, 98, doi: [10.1086/510378](https://doi.org/10.1086/510378)
- Riess, A. G., Rodney, S. A., Scolnic, D. M., et al. 2018, *ApJ*, 853, 126, doi: [10.3847/1538-4357/aaa5a9](https://doi.org/10.3847/1538-4357/aaa5a9)
- Rodney, S. A., Riess, A. G., Strolger, L.-G., et al. 2014, *AJ*, 148, 13, doi: [10.1088/0004-6256/148/1/13](https://doi.org/10.1088/0004-6256/148/1/13)
- Rubin, D. A., et al. in prep.
- Spergel, D., Gehrels, N., Baltay, C., et al. 2015, arXiv e-prints, arXiv:1503.03757. <https://arxiv.org/abs/1503.03757>
- Stauffer, J., Helou, G., Benjamin, R. A., et al. 2018, arXiv e-prints, arXiv:1806.00554. <https://arxiv.org/abs/1806.00554>
- Takada, M., Ellis, R. S., Chiba, M., et al. 2014, *PASJ*, 66, R1, doi: [10.1093/pasj/pst019](https://doi.org/10.1093/pasj/pst019)
- Vacca, W. D., Cushing, M. C., & Rayner, J. T. 2004, *PASP*, 116, 352, doi: [10.1086/382906](https://doi.org/10.1086/382906)
- Van Rossum, G., & Drake, F. L. 2009, *Python 3 Reference Manual* (Scotts Valley, CA: CreateSpace)
- Virtanen, P., Gommers, R., Oliphant, T. E., et al. 2020, *Nature Methods*
- Wolfram Research Inc. 2020, *Mathematica*, Version 12.1. <https://www.wolfram.com/mathematica>